Figure of merit for environmental SEM and its implications

Gerasimos D Danilatos

August 23, 2011

ESEM Research Laboratory, 28 Wallis Parade,
North Bondi, NSW 2026, Australia

Abstract

A recently introduced figure of merit for environmental and low vacuum scanning electron microscopes has now been computed in the full operational pressure range for one commercial instrument. The direct simulation Monte Carlo method has been used in lieu of experimental measurements. The theory of this figure of merit is further consolidated. It is shown that a thin pressure limiting aperture can indeed be used as an optimum reference system for all instruments employing differential pumping in the transfer of an electron beam from high vacuum to high pressure. The implications of the results obtained are discussed both in relation to existing commercial instruments and associated literature to pave the way for future progress in the field.

Introduction

This is a continuation in part of a previous report on the efficiency of electron beam transfer from the high vacuum of the electron optics column to the relatively high pressure environment of "low vacuum" and environmental scanning electron microscopes (LVSEM and ESEM) (Danilatos *et al.*, 2011). In the previous work, the direct simulation Monte Monte Carlo (DSMC) method (Bird, 1995) was employed to determine the gas flow field properties and, in particular, the gas density variation along the beam path. From this, the beam transmission was determined along the axis for various accelerating voltages and gas flow boundary conditions for some commercial instruments. Finally, a figure of merit for evaluating the instruments was devised and proposed. It is within the context of that report that the present paper must be read and reference to it is essential, although an attempt is made to keep the present report self-contained.

A thin pressure limiting aperture (PLA) was used as a reference standard for comparing the performance of various systems. One aim of the present paper is to provide further supporting evidence and justification for the use of a thin aperture as the standard optimum system by consolidating all the necessary information in various past reports and by additional new information not yet reported. Furthermore, the theory of the figure of merit is reviewed and expanded, and its computation in the full operational pressure range by the use of the DSMC method, ahead of experimental measurements, is provided for one instrument. It is anticipated that these findings may be confirmed, used and followed up with corresponding experiments by other users or makers of the instruments.

The implications of the present findings are further discussed in order to address a number of misconceptions that have found their way in the literature of ESEM, especially where this literature appears to reinforce practices that contradict past and present findings. The aim is to assist both the maker and the user in the creation and operation of a much better system than the ones currently in use.

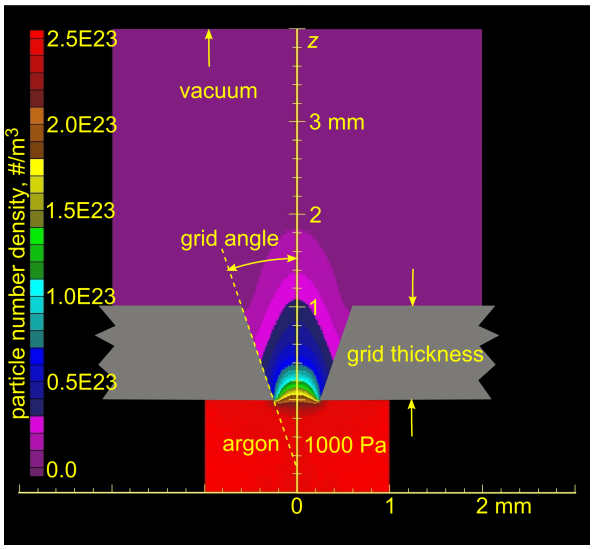

Figure 1: Parameters of orifice, grid angle and grid thickness with accompanying flood contours of density for argon flowing from a high pressure below to vacuum above.

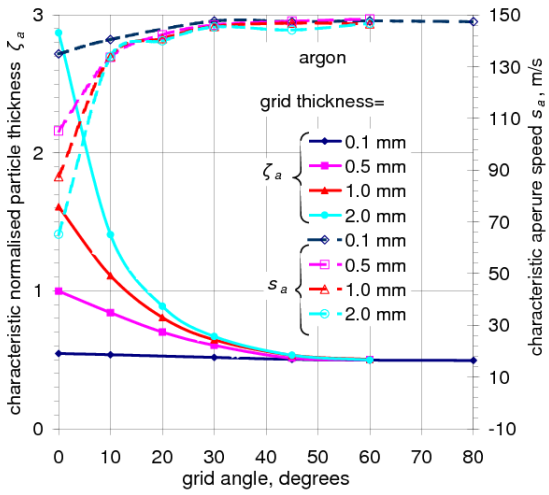

Figure 2: Effect of aperture grid thickness and angle on characteristic normalised particle thickness and aperture speed.

Figure of merit

A figure of merit has been devised and introduced for the purpose of evaluating the performance of electron microscopes that use a gaseous environment to some pressure level. It has been found that commercial ESEMs and LVSEMs incur unnecessary primary beam losses during the passage of the beam in the pumping stage prior to its entry in the specimen chamber. These excess losses are measured relative to the losses incurred by a thin pressure limiting aperture, which represents the best physically possible configuration in a conventional type of differential pumping system. The use of such a reference system was previously postulated in working out the figure of merit (Danilatos *et al.*, 2011). The validity of this assumption is now demonstrated by computational means in the next section. Below, we first review the background theory leading to this figure of merit.

To find the performance of a machine at any given accelerating voltage, we have a simple exponential decrease of the beam transmission f by:

$$f = \frac{I}{I_0} = exp\,(-m) \tag{1}$$

where I_0 is the initial beam intensity as it enters a gas layer of thickness L, and I is the intensity of the transmitted (un-scattered) beam current at the exit of the layer. The parameter m is the average number of scattering events with the gas particles (atoms or molecules) per electron and is given by

$$m = \sigma \int_{z}^{z+L} n(z)dz \tag{2}$$

where σ is the total scattering cross-section of the gas and $n(z)$ is the particle number density ($\#/\mathrm{m}^3$) along the axis z. Inside the specimen chamber and away from the effects of PLA on the gas flow, the latter function has a constant stagnation value n_0, from which we get simply $m = \sigma n_0 L$. However, elsewhere we require knowledge of the function $n(z)$. This is generally different for each machine, whilst it is unknown and relatively difficult to experimentally measure, as it varies over small distances of the order of aperture diameter, or over 10 or more mm in a region where access is usually not easy.

Since the scattering cross section is strongly dependent on the accelerating voltage used, to characterise the system we initially need only the average particle density $n(z)$ along the axis z in a cylinder with diameter equal to the diameter of the orifice. It is mostly inside this cylinder (especially at high magnifications) that the electron beam is scanned during imaging. As a consequence, the beam has to overcome the total number of gas particles per unit area q, which is found by the integral

$$q = \int n(z)dz \tag{3}$$

and which has been termed *particle-number thickness*, or *particle thickness*, for short. Because this function varies as the beam moves away from the axis, an average density is used from the values at three radii of 0.05, 0.1 and 0.15 mm.

We can use this parameter q alone to derive first the figure of merit for an instrument, whilst the actual beam transmission with its dependence on accelerating voltage can be derived from it as a second stage calculation. A specimen under examination is generally free to move inside the gaseous environment and thus there is a closest possible position to the PLA at which the total beam losses are minimal for any given machine. At this position, the particle thick-

ness is minimum and is designated as q_{min}. In a machine where the specimen can be imaged at **zero distance from a thin PLA exhausting in vacuum**, the corresponding minimum particle thickness is designated by q_c and is given by

$$q_c = \int_0^\infty n(z)dz \tag{4}$$

since it has been found that the integral converges to a finite limiting or critical value. In the next section, it is demonstrated that always $q_{min} \geq q_c$, i.e. q_c is an absolute physical minimum determined by the gas flow forming a jet downstream of the thin aperture plane exhausting in vacuum. Therefore, the difference $q_{min} - q_c$ is the excess particle thickness that the beam has to overcome and represents a measure of deviation from the absolute minimum set by the use of a thin aperture. If we also use the quantity q_c as a measuring unit of this difference, we arrive at a dimensionless factor ε

$$\varepsilon = \frac{q_{min} - q_c}{q_c} \tag{5}$$

that may be termed *excess particle thickness factor* and which can serve as a figure of merit for the given machine.

It is important to also introduce the main components of the excess particle thickness by the equation

$$q_{min} = q_{fore} + q_c + q_{aft} \tag{6}$$

where q_{fore} arises from the gas layer between the plane at the throat of the PLA and the specimen at the minimum distance, and q_{aft} arises from the gas layer added over and above the gas jet layer that would form by a thin aperture acting alone with its critical particle thickness q_c. The component q_{aft} can arise from inefficient removal of the gas that can be trapped in the pumping stage of the system, as will be shown by computations on a real machine later.

It is necessary to arrive at a generalised form of the same figure of merit so that computations of the properties of a thin aperture, once obtained, can be transferred to computations of any real machine. By partially normalising (dividing) the particle thickness first over the stagnation value of particle density n_0 in the specimen chamber

$$\theta = \frac{q}{n_0} \tag{7}$$

we derive the parameter θ that has been termed *stagnation gas thickness*. This has the dimensions of length and represents a gas layer at stagnation pressure (or density) with a particle thickness equal to the total particle thickness that is encountered by the beam. However, this normalisation means also that the same value of stagnation gas thickness represents different absolute values of particle thickness at different chamber pressures. With the latter caution, this is a useful parameter giving a tangible representation of the mass thickness of gas at any given chamber pressure.

In a similar fashion and assigning the same subscript designations, we can write the corresponding to Eq. 6 expression

$$\theta_{min} = \theta_{fore} + \theta_c + \theta_{aft} \tag{8}$$

Since from Eq. 7 we have

$$q = n_0\theta \tag{9}$$

we can obtain again the same figure of merit ε as

$$\varepsilon = \frac{\theta_{min} - \theta_c}{\theta_c} \tag{10}$$

which has been termed *excess stagnation gas thickness factor*.

Finally, by normalising the stagnation gas thickness over the diameter of the orifice D, we derive a dimensionless parameter, the *normalised particle thickness, or normalised thickness* ζ for short,

$$\zeta = \frac{\theta}{D} = \frac{1}{n_0 D}\int ndz = \frac{1}{n_0 D}\int \frac{p}{kT_0}dz \tag{11}$$

where we have also converted the number density n to pressure p from textbook gas theory with k being Boltzmann's constant and T_0 the absolute temperature of the gas in the chamber (here taken equal to 293 K).

Since from above we have

$$\theta = \zeta D \tag{12}$$

we are now ready to write the corresponding to Eq. 8 relationship using this dimensionless parameter as

$$\zeta_{min} = \zeta_{fore} + \zeta_c + \zeta_{aft} \tag{13}$$

where ζ_{min} is likewise the minimum normalised thickness of the total gas layer of the machine, ζ_{fore} is the corresponding component of normalised thickness before (or below) the aperture (if a given instrument imposes some physical obstruction to the specimen like the detector employed, etc.), and ζ_{aft} is the component when the said instrument imposes yet an additional gas layer after (or above) the aperture in excess to the inevitable critical value of ζ_c.

Therefore, the factor ε can be derived in an equivalent form as

$$\varepsilon = \frac{\zeta_{min} - \zeta_c}{\zeta_c} \tag{14}$$

which has been termed *excess normalised thickness factor*. We can then abbreviate all those three equivalent expressions, or terms, by the common name *epsilon* ε, which constitutes the figure of merit for any machine. This represents the amount of engineering inefficiency for an instrument, as the higher its value

the worse performance it has. The stipulation of the use of a thin aperture exhausting to vacuum together with the placement of a specimen at zero distance as a reference system is the topic of the following section and further discussion.

The figure of merit, as defined above, clearly depends on the aperture diameter and the gas pressure. The product of these parameters p_0D is proportional to the Reynolds number characterising all gas flows. It is a textbook knowledge from gas dynamics theory that different gas flows with the same Reynolds number are similar and it is sufficient to study one of these flows from which we can derive the values of corresponding parameters in any other flow. This principle has been employed in the measurement of the critical thickness ζ_c for various gases in the complete range of p_0D values from free molecule to continuum flow situations (that means in the complete range of pressures from low vacuum to one atmosphere as may be used in a generalised ESEM). The results of such work on ζ_c have been tabulated by Danilatos (2009) and can be used for the measurement of the figure of merit of any instrument. Therefore, the figure of merit ε should be provided as a function of p_0D in any practical range of operation, like

$$\varepsilon(p_0D) \geqslant 0 \quad with \quad (p_0D)_{min} \leqslant p_0D \leqslant (p_0D)_{max} \tag{15}$$

and defines the complete objective specification of the given instrument with regard to electron beam transfer.

As a second stage, from the above figure of merit, we can find the actual transmission efficiency at any pressure and accelerating voltage as follows. Let us call f_c the critical beam transmission of an optimum system, i.e. the transmission of beam up to the plane of a thin aperture exhausting in vacuum, and f_{min} the best beam transmission of a given instrument at the shortest possible (practical) working distance from its PLA. Then, we can define the *transmission efficiency* ε_f by

$$\varepsilon_f = \frac{f_{min}}{f_c} \tag{16}$$

A value of 1 means that the instrument has achieved the best possible transmission for the electron beam through the differential pumping system. We also obtain the following relationships:

$$f_{min} = exp(-m_{min}) = exp(-\sigma n_0 \theta_{min}) = exp[-\sigma n_0(\theta_\varepsilon + \theta_c)] \tag{17}$$

where

$$\theta_\varepsilon = \theta_{min} - \theta_c \tag{18}$$

is the *excess stagnation gas thickness*, so that

$$f_{min} = exp(-\sigma n_0 \theta_\varepsilon) exp(-\sigma n_0 \theta_c). \tag{19}$$

We also have

$$f_c = exp(-m_c) = exp(-\sigma n_0 \theta_c) \tag{20}$$

so that we finally obtain

$$\varepsilon_f = \frac{f_{min}}{f_c} = exp(-\sigma n_0 \theta_\varepsilon) = exp(-\sigma n_0 \theta_c \varepsilon) \tag{21}$$

by previous definition of ε and use of Eqs. 10 and 18. The last equation relates ε with ε_f and thus, from the figure of merit, we can derive the transmission efficiency and the actual transmission rate for any accelerating voltage and pressure p_0 (or n_0) of a given instrument.

Thick and thin aperture - optimum reference system

An orifice made on a thin wall and used to separate a pressurised chamber from vacuum has been postulated to provide the most abrupt transition from vacuum to a high pressure environment of any ESEM or LVSEM in all previous publications by Danilatos. Despite the obviousness of this postulate and despite all related publications, no commercial instrument has until recently employed it in practice. This necessitates now a detailed exposition of the same principle.

A most abrupt transition implies the minimum possible beam loss in the transition region from vacuum to high pressure. Any extra wall thickness clearly imposes an excess amount of beam loss. However, it should be mentioned also that a thicker aperture has a lesser conductance of the gas flow, which might have been seen as an advantage from the point of view of pumping requirements to achieve a good vacuum. On account of these conflicting requirements, we have prioritised the minimisation of beam loss over the pumping efficiency in any design, if the goal is to achieve the best imaging possible under the most favourable conditions. However, the value of this priority can be better seen if we concurrently quantify the two corresponding parameters, namely, the beam transmission and the amount of gas leaking through the aperture. Such detailed work has already been done in previous years but not yet published other than the use of the results as an obvious postulate in many related works. This was so especially in the absence of any claim that the thickness of an aperture has been deliberately used to minimise the leak rate and in the absence of any concomitant claim that the benefit of lessening the leak rate is preferable to the worsening of image quality on commercially available machines.

The gas flow properties through a thin aperture, as required in ESEM, were generally unspecified until the advent of the DSMC method together with present day powerful personal computers. In the free molecule flow, the aperture has been well studied

through the application of statistical mechanics. The continuum flow through converging-diverging (Laval) nozzles has also been studied well in the field of gas dynamics both experimentally and theoretically. However, a thin-wall orifice in the complete pressure range from free molecule to continuum flow was only partially understood or described analytically, or experimentally. Some properties have been measured experimentally, such as the flow rate (Liepmann, 1961), as well as some approximations of the density function in a limited range of Knudsen number (i.e. the ratio of mean free path over some representative physical length scale) of the flow (Ashkenas & Sherman, 1966; Beylich, 1984).

In search of an optimum differential pumping configuration, we can arrive at the use of a "thin" aperture as follows. We start with a "thick" orifice as is shown in Fig. 1. This is a specific example of the flow of argon starting with stagnation chamber pressure at 1000 Pa and flowing through an orifice with 0.5 mm diameter made on a wall thickness of 1 mm. The flood contours of the particle number density, in particles per cubic meter, are shown while the gas exhausts in vacuum. The number density differential created is more than two orders of magnitude in the span of about 4 mm above the bottom of the aperture grid that is exposed to the high pressure side. The inside rim of the orifice forms a 10^0 angle diverging in the direction of the flow so that the narrowest (throat) diameter is located on the high pressure side of the gas flow. The flow field has been computed with the DSMC method from which we can extract all the properties of interest at any point in the field like density, speed, Mach number, temperature, leak rate, etc.

By setting the lower limit of the integral in Eq. 11 at the throat (bottom) of the aperture (i.e. here coinciding with the axis origin at z=0 mm), the finite value obtained is a characteristic constant ζ_α for any given aperture:

$$\zeta_a = \int_0^\infty \frac{n}{n_0}\frac{dz}{D} \tag{22}$$

This characteristic normalised particle thickness ζ_α is plotted in Fig. 2 for different values of grid wall thickness and grid (divergence) angle. Most interestingly, we note that all curves converge very close to each other for grid angles greater than about 45^0. In the limiting case where either the grid thickness approaches zero or the grid angle approaches 90^0, the aperture attains a critical characteristic value ζ_c as defined and termed in the previous section. This condition can be used for the definition of a "thin" aperture, as was also proposed in previous reports (Danilatos, 2000, 2009; Danilatos *et al.*, 2011).

On the same graph, we also plot the corresponding *characteristic aperture speed* s_a, which is derived from the flow rate N of particles per unit time through the aperture

$$N = \iint n\upsilon \cdot dA \tag{23}$$

where υ is the velocity at the surface element dA having a number density n, with the integration taken over the area A of the aperture and, finally, by the equation

$$s_a = \frac{N}{n_0 A} \tag{24}$$

Likewise, in the limiting case where either the grid thickness approaches zero or the grid angle approaches 90^0, the aperture attains a critical characteristic speed s_c termed *critical aperture speed*. With this given, we can derive the flow rate for a thin aperture from:

$$N = s_c n_0 A = \frac{\pi s_c}{4kT} p_0 D^2 \tag{25}$$

or the leak rate Q in practical units of Pa.m^3/s used in vacuum technology according to the equation:

$$Q = kTN \tag{26}$$

The critical aperture speed for argon has been previously computed as a function of p_0D for a thin aperture in the complete range from free molecule to continuum flow (Danilatos, 2000), from which the same parameter for other gases was calculated via a proposed transformation formula. Since various gases have now been computed by the DSMC method and the critical normalised thickness has been published, the corresponding critical aperture speed magnitudes for the same gases are updated based on DSMC values and tabulated in the Appendix along with ζ_c retabulated for convenience and consolidation. Both parameters depend on the product of p_0D, any fixed value of which represents a family of equivalent flows for each gas, since this product is proportional to the Reynolds number. Both parameters are important in the design and construction of ESEM but the ζ_c takes precedence over s_c, because the primary aim is to transfer the electron beam with the minimum possible loss. A thick aperture clearly impedes the gas flow and the minimisation of leak rate is also important, but we should never sacrifice the beam intensity in order to save pumping capacity in any instrument. In a normal differential pumping system, the best way to minimise the leak rate is by the use of the smallest possible thin aperture, which also achieves minimum gas thickness at the same time. In fact, Fig. 2 demonstrates that with a grid angle of only 10^0, the leak rate has fast approached close to the maximum value attained with a thin aperture, whilst the gas layer thickness still remains significant. Therefore, there is no practical advantage in using a thick aperture, which has only the disadvantage of creating unnecessary beam loss. Hence, a thin aperture provides the ultimate choice for an optimum design and operation

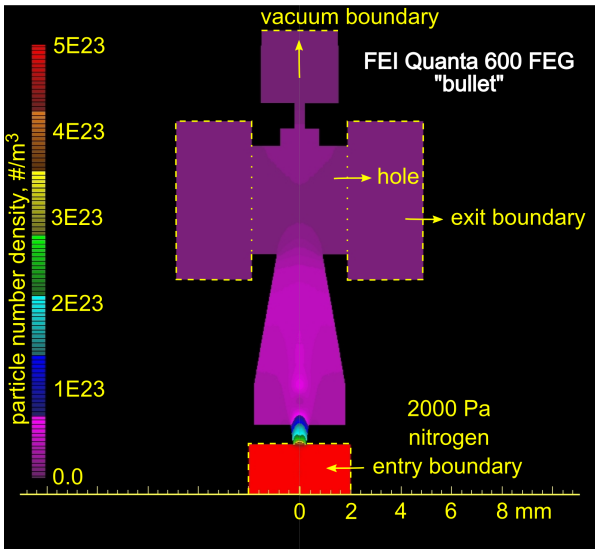

Figure 3: Geometry and flow field of nitrogen through the "bullet" of an ESEM. Flood contours show the number density variation in the field of the gas flowing from the specimen chamber below out through the exit holes in the tank and the vacuum of the column above.

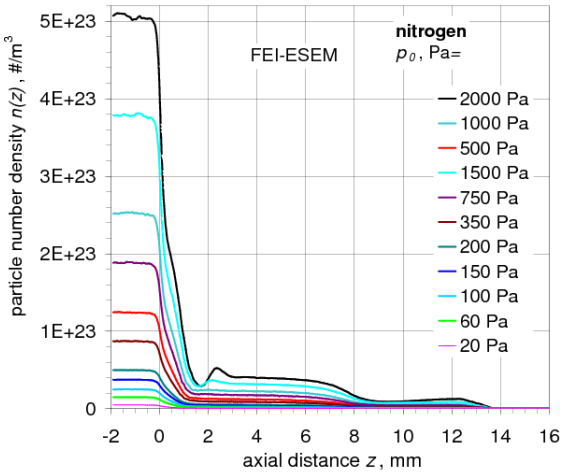

Figure 4: Variation of particle number density along the axis of the bullet at the fixed chamber pressures indicated for each curve.

of any ESEM. It is for this reason that it can be used as a reference system, against which the performance of any other design can be measured. Thus, we can stipulate that any microscope using a pressure limiting aperture should be capable of allowing the specimen to be imaged at zero distance from this aperture exhausting directly to vacuum. Although the number of useful applications with a specimen placed at zero distance from the aperture may be limited, this requirement sets a physical ultimate limit for any microscope.

Computation of the figure of merit by DSMC - real situation

The ultimate way to measure the figure of merit for an instrument is to experimentally determine (Rattenberger *et al.*, 2009) the electron beam transmission as a function of distance and pressure and then by use of the formula

$$\theta = \frac{m}{\sigma n_0} = \frac{mkT}{\sigma p_0} \tag{27}$$

to derive the required figure of merit from any of Eqs. 5, 10, or 14. Until this is conclusively done in the actual conditions of a laboratory, an alternative approach is available by the use of the DSMC method to compute the same, if the geometry and boundary conditions are known. The gas flow for one commercial instrument (the "FEI Quanta 600 FEG") operating either as an ESEM or as a LVSEM has been previously presented but only a few values were provided (computed) for ε (Danilatos *et al.*, 2011). We now extend the same approach in the complete range of operating pressures for both modes of its operation. Since the pressures were measured immediately outside the column downstream from the exit holes of the "bullet" and reported in the previous paper, we may use those values as the boundary pressure at the exit point of the holes. In reality, it is expected that the actual pressure at the exit holes should be somewhat greater than those measured values and the extent of deviation depends on the conductance of the path between the exit holes and the measured point. If the conductance is large, i.e. if the pathway is generally unobstructed, then the deviation should be very small or negligible. The amount of deviation may only be determined experimentally in the future, but the present work provides a firm basis and a guide for further comparisons, whilst, in the meantime, it represents the best possible performance for the particular instrument. Furthermore, the geometry at the PLA has now been determined more accurately by the use of an "*IFM*" imaging sensor by Rattenberger, who mapped the profile of the grid edge, according to Fig. 3, in which the grid thickness is found to be significant (760 μm) and the grid angle is small. This figure shows the details of the entire computed gas flow field as in previous work. The boundary at the exit holes that was used and discussed previously (Danilatos *et al.*, 2011) has now been shifted downstream to form the walls of a tank into which the exiting gas exhausts. Also, the boundary of the entering gas in the specimen chamber has been shifted further away (i.e. at 2 mm) from the PLA to eliminate any small effect from the flow close to the aperture. Therefore, the present simulation provides the best representation for the given instrument to date. By these new computations, it is confirmed that the gaseous boundaries used at present did not have any significant effect in comparison to

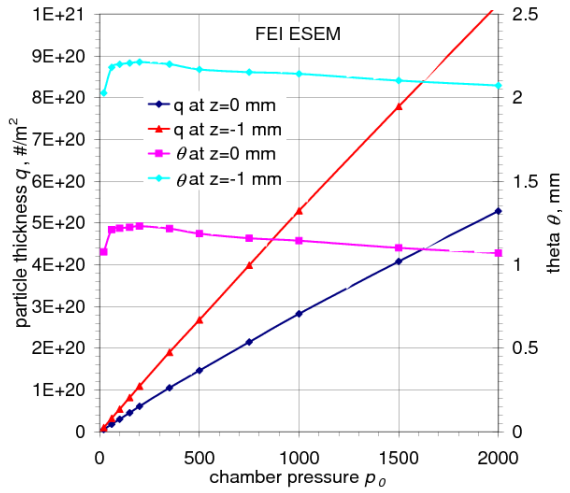

Figure 5: Variation of particle thickness and stagnation particle thickness versus chamber pressure.

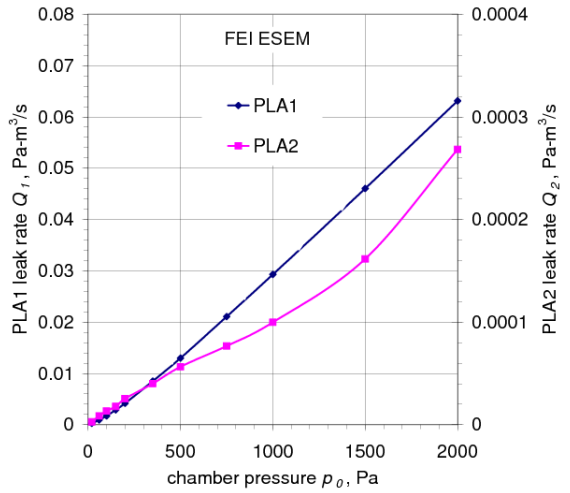

Figure 6: Variation of leak rate Q1 through PLA1 and Q2 through PLA2 versus chamber pressure.

the boundaries used in the previous publication and only the thickness and angle of the PLA has a deterioration effect according to Fig. 2.

We provide the results from such computations for the various parameters presented above. Fig. 4 shows the variation of average particle number density along the axis of the system for the fixed chamber pressures indicated with each curve. Fig. 5 shows the variation of particle thickness q and stagnation gas thickness θ against the chamber pressure p_0 for two cases of specimen positioning at z=-1 mm and z=0 mm. A closest specimen position reported has been at z=1.4 mm (Toth *et al.*, 2007), so that 1 mm is thought to represent a close to best practical position choice. At the same time, we include the "zero" distance for the hypothetical case of imaging at this distance also, for comparison purposes and parity with the reference "thin" aperture, although the existing detectors available do not normally allow imaging at this point.

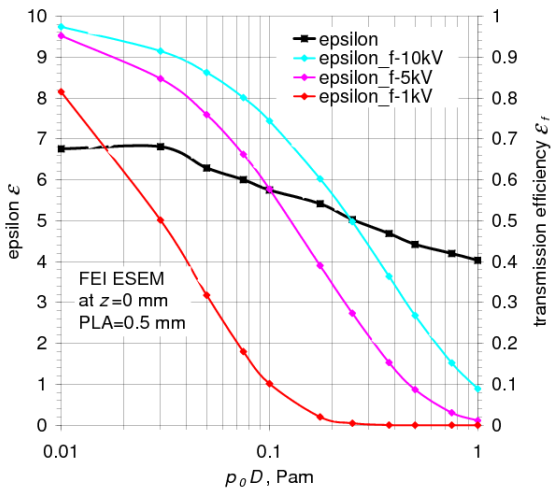

Figure 7: Figure of merit epsilon ε and transmission efficiency ε_f versus p_0D for three accelerating voltages at the minimum specimen position z=0 mm in the ESEM.

Next in Fig. 6, we present the absolute amount of gas leak rates Q_1 and Q_2 through either PLA1 or PLA2, correspondingly. Finally for the ESEM in Fig. 7, we present the epsilon ε and transmission efficiency ε_f for the case of specimen positioning at z=0 mm, because this represents the limiting case of all specimen positions; the user can determine the actual minimum specimen position and find the figure of merit from the provided curves in Fig. 4, for which it will generally be $\varepsilon_{actual} \gg \varepsilon_{zero}$.

In the same fashion, we also provide the results from such computations for the same parameters of the same instrument operating in the LVSEM mode. The flow field was already presented previously (Danilatos *et al.*, 2011) and is not repeated here because the use of "exhaust tank" as shown in Fig. 3 did not produce any measurable difference of any significance. Fig. 8 shows the variation of average particle number density along the axis of the system for the fixed chamber pressures indicated with each curve. Fig. 9 shows the variation of particle thickness q and stagnation gas thickness θ against the chamber pressure p_0 for two cases of specimen positioning at z=-9 mm and z=0 mm. Here, we have no information about the closest possible specimen position, which may be anywhere between -9 and 0 mm, although the latter position or close to it should be excluded on account of the type and detector position employed. We have included the "zero" distance, again, for the as yet hypothetical case of imaging at this distance also, for comparison purposes, although no such claim is known to be made by the maker, or any user. Next in Fig. 10, we present the absolute amount of gas leak rates Q1 and Q2 through either the throat (PLA1) or PLA2, correspondingly. Finally for the LVSEM in Fig 11, we present the epsilon ε and transmission efficiency ε_f for the case of

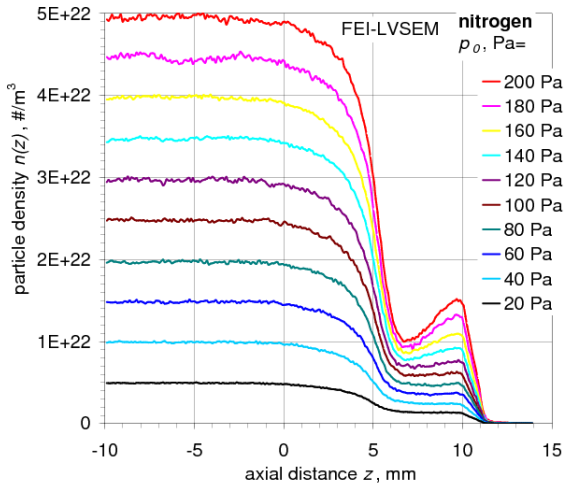

Figure 8: Variation of particle number density along the axis of the bullet at the fixed chamber pressures indicated for each curve.

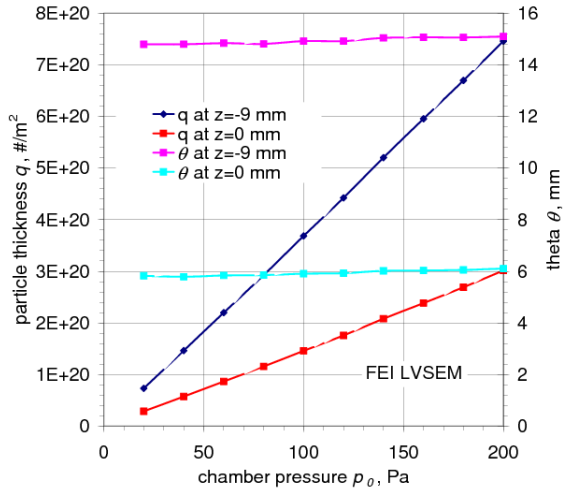

Figure 9: Variation of particle thickness and stagnation particle thickness versus chamber pressure.

specimen positioning at z=0 mm, because this represents the limiting case of all specimen positions; the user can determine the actual minimum specimen position and find the actual figure of merit from the provided curves in Fig. 8, for which it will generally be $\varepsilon_{actual} \gg \varepsilon_{zero}$.

Discussion

The figure of merit is a means to determine if and how much unnecessary loss of the primary beam is present in any given intrument design. Different instruments with the same figure of merit may not necessarily have the same specifications with regard to pressure range of operation. For example, two instruments both having $\varepsilon = 0$ can have very different pressure ranges depending on the size of PLA and the associated pump speed used. However, if these two

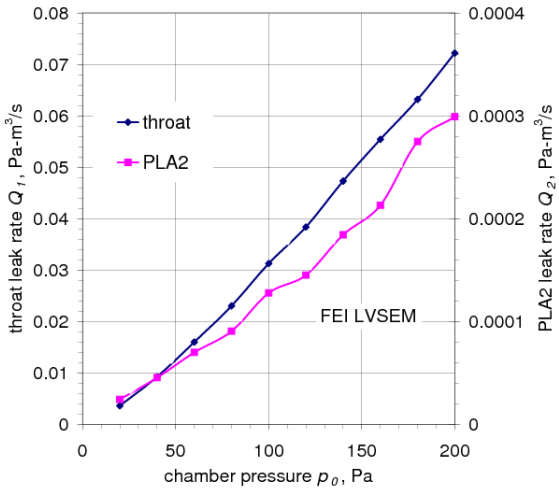

Figure 10: Variation of leak rate Q1 through PLA1 and Q2 through PLA2 versus chamber pressure.

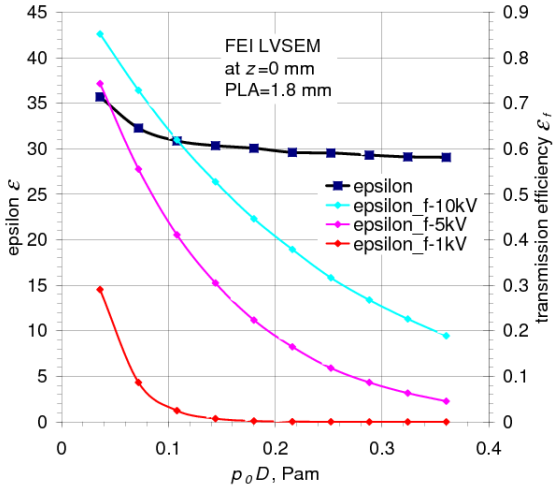

Figure 11: Figure of merit epsilon ε and transmission efficiency ε_f versus p_0D for three accelerating voltages at the minimum specimen position z=0 mm in the LVSEM.

instruments are designed to allow PLA size change with a given set of thin apertures, then they become equivalent if the associated pump speed is also the same. Beyond this similarity, the two instruments may differ in other regards, such as type of detectors and other important capabilities and specifications. Having established a figure of merit, the pressure range, in particular, is ultimately determined by Eq. 2 yielding the average number of scattering events per beam electron. By Eq. 1, the primary beam is extinguished exponentially leaving 5% of unscattered electrons when $m = 3$. This sets an upper limit of pressure in the oligo-scattering regime (defined by convention with $m \leq 3$) for ESEM operation as originally proposed by Danilatos (1988). The practical upper limit of the oligo-scattering regime is ultimately determined by the prevailing signal-to-noise ratio (SNR) in any given situation. Even in a "low vacuum" machine (LVSEM), it is easy to have a noisy image at low accelerating voltage with values of $m > 1$, which can overlap with the same values of m in ESEM at high pressure. As a consequence of all this, the hitherto distinction between LVSEM and ESEM is redundant and can be eliminated.

Although the graphs in Fig. 2 indicate that most of the variation of ζ_a and s_a occurs for grid angle less than 45^0 and grid thickness greater than 0.1 mm, there is still a small variation of ζ_a at grid thickness of 0.1 mm amounting to about 10%, which may be considered significant for work at very low accelerating voltage (e.g. 1 kV). Also, attention is drawn to the fact that the graphs represent the case of argon at 1000 Pa and that at different pressures the relative variation of the same parameters can be different. At much lower pressures, where the mean free path of the gas is much greater than the aperture diameter, there is a significant back diffusion of gas particles from the surface of the rim of the PLA, affecting the relative flow rate through the aperture. More importantly, for work at increased pressures, including atmospheric pressure, a thickness of 0.1 mm can be very detrimental to the point of making the system inoperable. Therefore, every effort should be made for creating a PLA with the sharpest possible edge. This problem has been solved in practice by the use of commercially available aperture grids having thickness less than 30 μm, in some cases down to 5 μm; there is no fear of collapse due to the force of pressure differentials, provided the design is based on tested practices (Danilatos, 1985). These grids can be mounted flat or bent to form a saddle around a ridge on a cup fitted below the pole-piece. The latter configuration has allowed the fitting of wedge shaped optimum BSE detectors (Danilatos, 1985), as it can also allow x-ray and other detectors to operate optimally in the ESEM. In fact, even for better results, conical geometry PLA can be made and supplied by industries specialising in the construction of skimmers used in molecular beam technology.

Figs. 6 and 10 indicate that the amount of leak in the upper column is at least two orders of magnitude less than the amount exhausting from the exit holes of the bullet, which is a satisfactory result.

The plotting of ε versus p_0D will generally produce a different curve for every change of D, because by changing only the diameter of the aperture, while keeping the rest of the flow geometry the same, it does not produce a similar overall flow field. The principle of similitude would apply for different pairs of pressure-diameter only in the range of pressures where the gas flow is entirely controlled by the aperture alone and not by the remainder geometry and the pumping efficiency of the given machine. The principle of similitude would be applicable to the entire gas flow system, if the entire system geometry was changed inversely to the pressure. In practice, the principle of similitude can be achieved with small enough and thin-apertures, which effectively control the flow irrespective of the remaining geometry; effectively, the gas exhausts to vacuum after it passes the thin aperture, i.e. in the range of p_0D, whenever ε is close to the zero value. Therefore, the curves of figure of merit should generally be accompanied by the size of PLA diameter used (as in the present case D=0.5 mm), on which it depends, in addition to its dependence on p_0D. By virtue of the above rationale alone, the figure of merit of the same instrument can be improved by the use of an ever smaller diameter PLA until ε is close to zero.

The definition of the optimum condition by imaging at zero distance from a thin aperture does not imply that all such work should be done at this point. This is just a physical limit of operation of any differentially pumped electron microscope. Most applications may require that the specimens be placed away from the streaming effects of the gas near the PLA, so that they must be placed at least one or two diameters distance from the aperture. However, we can still envisage a significant number of applications at lesser distances down to almost zero value, which makes it a rational choice for creating an optimum reference system at that point. In fact, imaging of specimens placed at the tip of a fine wire even through and above the PLA has been and can be done, but these may constitute a much smaller set of applications, with which no well defined limit may be assumed.

Based on the above findings and Fig. 3, not only the entire bullet geometry is inefficient (see also Danilatos *et al.*, 2011), but also the detailed geometry of the PLA itself (with 760 μm thickness and about 10^0 angle). This aperture geometry is responsible for a significant component of the electron beam loss that can be eliminated by simply replacing the provided thick grid with a commercially available thin copper grid (also disposable and inexpensive), but always adhering to the tested practices in the literature. Furthermore, should the user have the option of easily replacing the aperture grids with different diameter

hole, then the instrument could be made quickly far superior in performance. That is, by simply using a much smaller than the now fixed 0.5 mm PLA, the pressure could be significantly increased and the image signal-to-noise ratio vastly improved. That possibility would only limit the field of view at low magnifications for the existing instruments, but this is a minor sacrifice that most users could accept in order to achieve the greater benefits at high magnifications, without forfeiting the option of reverting to a large PLA. Actually, the field of view needs not be sacrificed, if the instrument were to incorporate the relocation of the rocking point of the beam close to or at the PLA1, which would allow a very large field of view even with the use of very small PLAs including sizes of 100 μm and even 50 μm (Danilatos, 2004). Instead, the minimum size of a rather thick PLA appears invariable by the industry to only 0.5 mm diameter (Stokes, 2008) for a long time, for some hitherto arbitrary reason.

The fact that such simple or obvious as above kind of solutions exist but are not yet implemented, even after 20 years of commercialised ESEM, is rather extraordinary. Furthermore, the fact that a large number of publications have emerged from the use of those instruments without addressing the actual problems has created a peculiar situation. This has now necessitated the introduction of a figure of merit (i.e. a new study of inefficiency) to explain the phenomena in the hope to rectify the technology. The figures of merit plotted in Figs. 7 and 11, demonstrate that both modes of this instrument operate far away from the optimum condition. In fact, the LVSEM mode is relatively worse than the ESEM mode, presumably because it may have been assumed that the "low vacuum" is quite safe to operate, without regard to the actual beam loss. It may be due to relying more on un-confirmed assumptions than on rigorous quantitative analysis of the system. This implies that a review of some published works is needed, especially of those that have contributed to a misunderstanding of the purpose and capabilities of ESEM and, in particular, of those connected with the industry. To this end, an attempt is made in the following sub-section to highlight some of the outstanding issues.

Implications

To start with, the figure of merit in the two modes of operation of the presented instrument has been computed for a hypothetical best situation by placing the specimen at z=0 mm, which is not actually accessible by either mode; hence, the actual case should be even worse. An insight of the actual situation can be gained by quoting from an article by Toth, Uncovsky and Knowles (2007) (FEI authors), who state that "*in practice, the maximum pressure employed in ESEM is limited by a decrease in image quality with pressure (at pressures greater than 500 Pa). Consequently, high pressure imaging necessitates the use of high beam currents, giving rise to low resolution (due to electron optical aberrations)[12] and rapid degradation of beam sensitive materials. Here we demonstrate high quality secondary electron (SE) imaging at high pressure (2 kPa), using a relatively low beam current (70 pA). This is achieved by optimizing boundary conditions that govern electron beam scatter in the gas, the energy distribution of low energy electrons traversing the gas, dielectric breakdown of the gas, and electron detector collection efficiency. High pressure ESEM will enable imaging of hydrated materials at close to room temperature (17 °C), and surface modification processes occurring at high pressures. Experiments were performed using a FEI Quanta field emission gun ESEM, using the sample-detector geometry shown in Fig. 1. The electron beam enters the high pressure specimen chamber through a conical pressure limiting aperture (PLA)*". However, this statement does not take into account the fact that pressures close to 7 kPa were already achieved by 1979 (Danilatos & Robinson) and one atmosphere (100 kPa) by 1980 (Danilatos) routinely operating at room temperature.

The above quotation claims an improved, even optimised system while, in reality, departs from prior successful practices in the literature. The flat cup of the PLA1-detector fitted at the bottom of the bullet is simply replaced by a conical cup protruding below the bottom of the **same** bullet. Actually, the user can interchange the flat or protruding cups at will. This allows the user to approach the specimen at much closer distance with the conical cup protruding further below the pole-piece than the minimum distance allowed by the flat cup. However, by doing so, the travel distance of the beam between PLA1 and PLA2 increases accordingly, because the bullet remains the same. The inside angle of the cone and the precise geometry of the PLA1 at the bottom of the cone are not provided. At any rate, the beam loss between the two apertures is greater in the extended conical system described and hence no improvement is possible over and above that provided by the figure of merit plotted herewith for a flat cup. Thus, an improvement is gained by placing the PLA closer to the specimen (i.e. by making the term θ_{fore} smaller), but a concomitant deterioration is also caused by increase of the term θ_{aft}. From the same reference, we see that the minimum "*sample-PLA gap=1.4 mm*". Therefore, the 1 mm used in the present work is a generous choice for plotting the minimum stagnation gas thickness in Fig. 5, along with the minimum particle thickness. For any longer specimen distance, the added gas layer is homogeneous (at stagnation density) and the reader (user) can easily deduce the actual figure of merit and the beam loss for this particular commercial ESEM.

In the same reference above, a "*needle*" detector in conjunction with the conical aperture is used to make secondary electron (SE) images at high pressures in

excess of 1 kPa. However, formation of SE images at high pressure should not be necessarily linked with a differential system that proves to also incur high beam losses, nor a ring-shaped anode should be excluded from generating SE imaging at high pressure. Hence, caution is required in stating that "*finally, we note that many ESEM systems use a gaseous SE detector with a ring-shaped anode [1] for SE imaging at pressures in the range of ∼150–600 Pa. This configuration is unsuitable for imaging at greater pressures because the electric field generated by such an anode is very inefficient at extracting SEs when the PLA-sample gap is as small as needed for imaging at pressures in excess of ∼1 kPa.*" Notably, the needle detector had already been disclosed by Danilatos (2004) (patent priority date August 2000, claims #14+), also earlier mentioned in a comprehensive theory of the gaseous detection device (Danilatos, 1990) and "in some critical issues of ESEM" (Danilatos, 1993a), to all of which there is no reference. Also, the conical-aperture/specimen system had already been studied with the DSMC method and reported in detail by Danilatos (1992), to which there is no reference either. There is only one relevant reference by stating that "*the extent of beam scatter is given by the product of pressure and beam path length in the gas [16]. The latter is minimized by placing the PLA close to the sample surface, as is shown in Fig. 1, where we used a sample-PLA gap of 1.4 mm.*" Reference [16] is attributed to Danilatos, but with no mention that the paper deals with the much more important topic of electron beam loss **inside the bullet** by the use of DSMC method, in the same way as is done in the present paper. In summary, the images shown were taken at 30 kV with dwell time =300 μs / pixel, both of which remain very high, whilst the use of accelerating voltages well below 5 kV, down to 1 kV, at much shorter recording times, as predictable by the present report, have remained well outside the reach of microscope used by the authors above.

One year later, Stokes, Chen, Neijssen, Baken and Uncovsky (2008) (FEI authors) have repeated the same theme, as they state again that "*so far, imaging of hydrated materials has required cooling of the sample to just above freezing to achieving adequate high humidity within the pressure range of a gaseous secondary electron detector. In practice, the maximum gas pressure is physically limited by an increase in primary electron beam scattering, and hence a decrease in image quality, at elevated pressure (i.e. pressures greater than ˜600 Pa). Hence high pressure imaging requires the use of high beam currents, which increases the beam diameter, limiting the resolution. However, with the recently introduced, commercially available, High Pressure detector for the ESEM, it is possible to get high quality secondary electron (SE) imaging at high pressures (in the kilopascal regime), using a relatively low beam current (sub-100 pA). This is achieved by optimizing boundary conditions that govern electron beam scattering in the gas, the energy distribution of electrons in the gas cascade, dielectric breakdown of the gas and detector collection efficiency [1]*" with reference [1] being to previous Toth *et al.* (2007). However, such an "optimising of boundary conditions" is nowhere near the optimisation reported in the present paper and the claim that "*the latest systems offer un-compromised performance over an unprecedented range of sample chamber vacuum conditions*" is not in accord with preceding historical facts.

Identical claims in relation to high pressure and room temperature use in ESEM had been previously made also by Stokes-Baker-Toth (2004), again by Stokes (2006) and again by Stokes-Baken (2007). Again. none of those works mention the works done both at high pressure and room temperature by Danilatos who, in fact, has consistently avoided the cooling of specimens throughout all his ESEM papers.

The ideas quoted above have been further consolidated in a latest book by Stokes (2008) that contains areas covered by the findings in the present paper. For example, instead of using the concept of stagnation gas thickness, or number thickness, or normalised thickness of the gas responsible for all the beam losses, we only see the geometrical distance between specimen-PLA being considered: The "*gas path length*" (GPL) is clearly defined as the distance between specimen and PLA (see Fig. 4.1, p. 96 in the book). A protruding aperture below the pole piece (some form of tube in Fig. 4.11, p. 112) to reduce GPL is advocated once more, but again there is no mention to what happens above the PLA. There is, however, only a fine print short footnote (p. 111) that "*Inevitably, a small number of gas molecules will give rise to scattering even before the primary electrons enter the aperture or extension tube, but their effect is negligible under the circumstances discussed here*". Therefore, the serious beam loss occurring above the PLA has been bypassed. At the same time, Stokes and co-workers appear to be setting the "*roadmap*" for later instrument designs in Fig. 1.3 of the same book. This appears to have been a different roadmap from the one based on the findings in the present paper, or many previous works in the span of the last 30 years, or more. The difference is both significant and critical, because one road terminates prematurely with artificial beam barriers, whilst the other leads us all the way to the ultimate limits imposed only by nature itself. This becomes further evident by the following quoted example from the book: "*4.5 HOW MUCH GAS? 4.5.1 Introduction. The pressure range in the VP-ESEM can be varied from about 10 Pa up to 2660 Pa (20 torr)... (p. 114:) We now consider the elastic scattering of primary electrons as a function of pressure over a range of primary electron beam energies, for 5keV* $\leq E_0 \leq$ *30 keV... (p. 120:) As predicted earlier (Section 4.5.2.1), the fraction of focused electrons remains relatively high for*

beam energies above 10 keV and pressures of a few hundred pascals. For energies around 5 keV, formation of a focused probe is highly unlikely at the highest pressure, but still possible for high energies." Such an understanding is definitely consistent with and is confirmed by the present results on the FEI machine. Therefore, the range of accelerating voltages below 5 kV have admittedly remained outside the reach of those instruments, while the overall performance is far removed from real optimum capability at all accelerating voltages and environmental conditions.

There is also an attempt to coin a new term like "VP-ESEM" that might presumably include the LVSEM (a similar attempt made also by Griffin (2007)). The separation between ESEM and LVSEM has arisen from the inability of certain commercial machines to accommodate higher pressures on the same machine for various reasons, for which they coined different and separate names. Objectively, such a separation has been unnecessary. A low vacuum mode operating, say, up to around 200 Pa, can be easily switched to an ESEM operating, say, at around 600 Pa by simply replacing the PLA by a smaller diameter approximately inversely proportional to the factor $\sqrt{600/200} = 1.73$. This reality is a corollary of the present and past reports. There is no objective (i.e. physical or scientific) justification why the maker or the user cannot provide such a simple option. "Gaseous" SEM could, perhaps, be more descriptive than the arbitrary and longer wording "variable pressure", or "natural", "wet", etc. (terms introduced only to differentiate different makes of machines with essentially the same capability). Since ESEM really embraces all modes of gaseous operation, its defacto generic name should require no replacement. However, if a search for a unifying name must be done, then all previous proposals should be considered including the "universal ESEM" that embraces both LVSEM and vacuum SEM (Danilatos, 1993b). In the end, real instrument progress should precede any need for a new name, not the reverse.

The undertaking at the outset of the book that "*the principles and applications have been outlined in a generic way, applicable to readers familiar with any of the types of VP-ESEM on the market, irrespective of manufacturer*" does not explain why the descriptions of ESEM are so closely linked with the limitations of one particular machine. The limits provided for an ESEM constrained by a minimum size of PLA fixed at 0.5 mm is just one example. Another is the need to cool the specimen in that machine, which is a direct consequence of the excess primary beam loss that is ameliorated by the low saturation vapour pressure near the freezing point. The localised lowering of specimen temperature makes the achievement of a steady stagnation chamber pressure prolonged and complicated on account of variable temperature between specimen and PLA. The situation becomes further complicated and problematic during specimen transfer from ambient conditions to the ESEM environment. The book dwells on "*one way... through 'purge–flood' cycles*", which was introduced by Cameron & Donald (1994) and adopted by the manufacturer as standard procedure for general use. This method was devised specifically to remedy the effects of harsh dynamic pumping of a large volume of the chamber on this machine, instead of the alternative proven specimen exchange chamber (airlock) successfully practiced and proposed by Danilatos (1988, p. 238+) from the outset of experimental ESEM work. With continuous supply and direct pumping of chamber gas, the condition of stagnation equilibrium is difficult or never achieved, whilst the solution of an airlock, already available in generic ESEM, has received no mention. The total effects of these and other practices define the limits, under which work is reported both in the book and other literature having used a similar machine. The conclusions by many of those applications may have to be re-considered when better ESEM machines become available, since the operational limits have been narrowed down by the excess beam loss during its transfer from vacuum to the specimen chamber.

Conclusion

A figure of merit previously devised has been computed in the full pressure range for one commercial ESEM and found that there is room for many improvements. It is possible to extend the pressure range upwards and the accelerating voltage downwards, well beyond the existing limits of some instruments. It is possible to operate the ESEM at room temperature routinely and cool the specimen only if there is a special requirement. These and other constraints must be removed. At the same time, performance by way of image quality, specimen integrity and ease of operation can be greatly improved. Progress in this direction is well overdue, since it has been promised for the most part of the last 30 years of research and development.

The figure of merit should be provided with each commercial machine, or users should be equipped to measure it and report it for their own benefit and others. This can be found either by experimental measurements or by DSMC computations given the boundary conditions of the gas flow, or a combination of experimental measurements and computation as appropriate.

The implications of the introduction and use of a figure of merit should result also in the critical study of published literature and in a more rigorous approach to further work and publications in the field of ESEM. It is hoped that the present report will contribute towards the manufacture of a much improved electron microscope involving the use of a gaseous environment.

Acknowledgment

The geometrical details of the "FEI Quanta 600 FEG" bullet and the pressure measurements of the pumped gas at the column outlet have been kindly provided by J. Rattenberger from the Institute for Electron Microscopy, Graz University of Technology/Centre for Electron Microscopy Graz, Austria.

References

Ashkenas, H. & Sherman, F.S. (1966) The structure and utilization of supersonic free jets in low density wind tunnels. In J.H. de Leeuw, ed., *Proc. 4th Int. Symp. on Rarefied Gas Dynamics*, vol. II, pp. 84–105. Academic Press, New York, London.

Beylich, A. E. (1984) Plane flow through an orifice. In Hakuro Oguchi, ed., *Proceedings 14th Int. Symp. on Rarefied Gas Dynamics*, pp. 517–524. University of Tokyo Press, Tokyo.

Bird, G.A. (1995) *Molecular Gas Dynamics and the Direct Simulation of Gas Flows*. Oxford University Press, New York.

Cameron, R.E. & Donald, A.M. (1994) Minimising sample evaporation in the environmental scanning electron microscope. *J. Microsc.* **173**, 227–237.

Danilatos, G., Rattenberger, J. & Drakopoulos, V. (2011) Beam transfer characteristics of a commercial environmental SEM and a low vacuum SEM. *J. Microsc.* **242**, 166–180. Submitted.

Danilatos, G.D. (1980) An atmospheric scanning electron microscope (asem). *Scanning* **3**, 215–217.

Danilatos, G.D. (1985) Design and construction of an atmospheric or environmental SEM (part 3). *Scanning* **7**, 26–42.

Danilatos, G.D. (1988) Foundations of environmental scanning electron microscopy. *Advances in Electronics and Electron Physics, Academic Press,* **71**, 109–250.

Danilatos, G.D. (1990) Theory of the gaseous detector device in the ESEM. *Advances in Electronics and Electron Physics, Academic Press,* **78**, 1–102.

Danilatos, G.D. (1992) Gas-flow field in the environmental SEM. In G.W. Bailey, J. Bentley & J.A. Small, eds., *Proc. 50th Annual Meeting EMSA*, vol. II, pp. 1298–1299. San Francisco Press, San Franciso, CA, USA.

Danilatos, G.D. (1993a) Environmental scanning electron microscope-some critical issues. *Scanning Microscopy International, Supplement 7* **1993**, 57–80.

Danilatos, G.D. (1993b) Universal ESEM. In G.W. Bailey & C.L. Rieder, eds., *Proc. 51st Annual Meeting MSA*, pp. 786–787. San Francisco Press, San Francisco, CA, USA.

Danilatos, G.D. (2000) Direct simulation monte carlo study of orifice flow. In T.J. Bartel & M.A. Gallis, eds., *Rarefied Gas Dynamics, 22nd Intern. Symp.*, vol. 585, pp. 924–932. American Institute of Physics, Sydney, Australia.

Danilatos, G.D. (2004) Environmental scanning electron microscope. *United States patent* **6809322**.

Danilatos, G.D. (2009) Optimum beam transfer in the environmental scanning electron microscope. *J. Microsc.* **234**, 26–37.

Danilatos, G.D. & Robinson, V.N.E. (1979) Principles of scanning electron microscopy at high specimen pressures. *Scanning* **2**, 72–82.

Griffin, B.J. (2007) *Electron Microscopy: Methods and Protocols*, vol. 369 of *Methods in Molecular Biology*, chap. 23 Variable pressure and environmental scanning electron microscopy: Imaging of biological samples, pp. 467–495. Humana Press, Inc., Totowa, N.J., USA.

Liepmann, H.W. (1961) Gas kinetics and gas dynamics of orifice flow. *J. Fluid Mech.* **10**, 65–79.

Rattenberger, J., Wagner, J., Schröttner, Mitsche, S. & Zankel, A. (2009) A method to measure the total scattering cross section and effective beam gas path length in a low-vacuum SEM. *Scanning* **31**, 1–7.

Stokes, D.J. (2006) Progress in the specimen using study of biological ESEM. *Proceedings of Royal Microsc. Society* **2**, 64–72.

Stokes, D.J. (2008) *Principles and Practice of Variable Pressure/ Environmental Scanning Electron Microscopy (VP-ESEM).* John Wiley & Sons, Ltd., Chichester, U.K.

Stokes, D.J. & Baken, E. (2007) Electron microscopy of soft nano-materials, imaging in the native state. *G.I.T. Imaging & Microscopy* **02**, 17–20. (GIT VERLAG GmbH & Co. KG, Darmstadt, Germany).

Stokes, D.J., Baker, F.S. & Toth, M. (2004) Raising the pressure: realizing room temperature/high humidity applications in ESEM. *Microscopy and Microanalysis* **10**, 1074–1075.

Stokes, D.J., Chen, W.A.J, J. and. Neijssen, Baken, E. & Uncovsky, M. (2008) High pressure imaging in the environmental scanning electron microscope (ESEM). In *14th European Microscopy Congress, Aachen, Germany*, pp. 627–628. Springer, Heidelberg-Berlin.

Toth, M., Uncovsky, M. & Knowles, R.W. (2007) Secondary electron imaging at gas pressures in excess of 1 kpa. *Applied Phys. Letters* **91(053122)**, 1–3.

Appendix

The characteristic aperture speeds for various gases obtained by the DSMC method are presented below for the first time, while they were obtained simultaneously with the critical particle thickness already reported but also included below for completeness and convenience. The critical thickness for each gas can be satisfactorily fitted with a function of the form

$$y(x) = \frac{1 + bx + dx^2}{a + cx + ex^2} \tag{28}$$

where $\zeta_c \equiv y(x)$ and $p_0 D \equiv x$, and the constants a, b, c, d and e are given in Table 1. Similarly, the same form of fitting function has been used for the corresponding critical speeds s_c in Table 2, where $s_c \equiv y(x)$ and $p_0 D \equiv x$.

The form of both parameters is a generally sigmoid shape varying from a low constant value to a high constant value with a small "hump" before the high value. For the critical particle thickness, the low value in the free molecule regime is a universal constant for all gases $\zeta_{c1} = 0.25$ that has been theoretically derived by Danilatos (2000), whilst the computed value is a little lower due to the finite thickness of the orifice used . The high value in the continuum flow regime is another constant that depends on the nature of gas. In the transition regime, values vary according to the fitting equation above.

The low value for the critical speed of an infinitely thin aperture can be derived theoretically in the free molecule flow as (see any vacuum technology book, or in Danilatos (2000)):

$$s_{c1} = \sqrt{\frac{RT_0}{2\pi M}} \tag{29}$$

where R is the universal gas constant and M the molecular weight of the gas. It is found that the theoretical values are between 3.5-6.5% higher than the computed values in this work, which may be attributed to the small fraction of molecules that are back diffused from the finite thickness of 0.1 mm used; the theoretical low value has been achieved also with the DSMC method by the use of a much thinner aperture and by shifting the entry boundary of the computed flow to many diameters away from the aperture (Danilatos, 2000). A corresponding theoretical formula in the continuum flow for the maximum constant value of the speed is that provided for the isentropic flow though a Laval nozzle:

$$s_{c2} = \sqrt{\frac{\gamma RT_0}{M} \left(\frac{2}{\gamma + 1}\right)^{\frac{\gamma+1}{\gamma-1}}} \tag{30}$$

where γ is the specific heats ratio. It is found that this formula gives a significantly higher value than the computed values for a thin aperture herewith (e.g. 20% higher for argon). This is to be expected since both a boundary layer at the rim of the PLA together with a vena contacta formed result in an effective nozzle with a smaller diameter than the PLA used. This has made it difficult to derive an analytical formula that quantitatively describes the flow of compressible gases through a thin aperture in the continuum and transition regimes (Danilatos, 2000).

The tabulated values can be revised with even better precision as programs are written for the DSMC to run on 64 bit computers in the future.

Table 1: Constants of Eq. 28 for the critical normalised thickness ζ_c for various gases.

Gas	a	b	c	d	e
Argon	4.0915478	23.505763	45.923236	1.314958	0.02925647
Helium	4.1206162	11.647015	29.843766	24.269588	47.500051
Hydrogen	4.096053	73.238737	281.12711	1212.3227	2752.7335
Neon	4.0225785	9.7785397	20.26494	11.738297	23.605902
Nitrogen	4.055408	23.323677	54.013017	147.32355	350.43078
Oxygen	4.0627935	24.024988	55.630753	90.879174	215.09807
Water vapour	4.039353	26.117061	60.680093	28.194384	72.345331

Table 2: Constants of Eq. 28 for the critical aperture speed s_c for various gases.

Gas	a	b	c	d	e
Argon	0.01070795	27.43347	0.17738715	4.1413311	0.02925647
Helium	0.00335459	8.8228082	0.01862066	25.429723	0.05432455
Hydrogen	0.00240630	0.81859927	-0.01495783	-334.69728	-0.50304835
Neon	0.00771832	17.782559	0.08238812	20.147081	0.09635782
Nitrogen	0.00886153	27.867948	0.15348754	235.85886	1.3852781
Oxygen	0.00955098	37.451249	0.22632365	-4.6904792	-0.02646638
Water vapour	0.00741718	51.565748	0.24890498	54.57068	0.2791621